Catalysis Today 139 (2008) 119–124

Contents lists available at ScienceDirect

Catalysis Today

journal homepage: www.elsevier.com/locate/cattod

Microwave electrodeless lamp assisted catalytic degradation of X-GRL with manganese dioxides: Adsorption and manganese(IV) reductive dissolution effects

Ruiping Liu [a], Hongjie Wang [a,b], Xu Zhao [a], Shuhu Xiao [a,b], Jiuhui Qu [a,*]

[a] Research Center for Eco-Environmental Sciences, Chinese Academy of Sciences, Beijing 100085, PR China
[b] Graduate School, Chinese Academy of Sciences, Beijing 100039, PR China

ARTICLE INFO

Article history:
Available online 2 October 2008

Keywords:
X-GRL
δMnO_2
βMnO_2
Adsorption
Reductive dissolution
Catalysis
Microwave electrodeless lamp

ABSTRACT

This study focuses on the adsorption and microwave assisted-oxidation of Cationic Blue (X-GRL) on hydrous manganese oxides (δMnO_2) and commercial MnO_2 (βMnO_2). The effects of X-GRL adsorption and Mn(IV) reductive dissolution are investigated. δMnO_2 exhibits higher adsorbing potential for X-GRL than βMnO_2 does, with dissolved organic carbon (DOC) removal potential (removed DOC at per gram MnO_2) of 4.92 and 0.31 mg/g, respectively. The ratio of absorption at different wavelength ($A_{202\ nm}/A_{300\ nm}$/$A_{610\ nm}$) and ratio of DOC to $A_{610\ nm}$ ($R_{DOC}/A_{610\ nm}$) varies after adsorption. This implies the electron transfer between manganese oxides surfaces and X-GRL, which is confirmed by dissolved Mn(II) concentration increase. δMnO_2 exhibits more remarkable oxidizing effect than βMnO_2 does. X-GRL adsorption onto δMnO_2 involves in hydrogen bonding and electrostatic interactions, which is inhibited by Ca^{2+} presence and favored at higher pH. Manganese species (δMnO_2, βMnO_2 and Mn^{2+}) facilitates X-GRL degradation and DOC removal in O_2/MWL systems, and more significant effects are observed for δMnO_2 due to its combined effects of adsorption and catalysis. The k_{app} (apparent reaction constant) in the initial 10 min with δMnO_2 presence is about 2.5 and 4.2 times higher than that with βMnO_2 and Mn^{2+} presence, respectively. However, with reactions continuing, DOC mineralization is inhibited in heterogeneous systems due to the adverse effect of high dissolved Mn^{2+} concentration.

1. Introduction

The catalytic process assisted with microwave (MW) lamp has received attention in the past years. Kataoka et al. [1] reported that microwave led to much faster oxidation rate as 83.9% for photodegradation of ethylene. Horihoshi et al. [2] demonstrated that MW irradiation contributed to the formation of 20% more $^{\bullet}OH$ radicals. Zhang et al. [3] showed that the UV–vis light and MW irradiation exhibited excellent capability for acid orange 7 decolorization and mineralization, and demonstrated the formation of oxidative species (e.g., $O_2^{\bullet-}$, $^{\bullet}OH$, H_2O_2 and O_3). Inorganic oxidizing species as O_2, H_2O_2 and $Na_2S_2O_8$ enhanced pollutants degradation in MW/UV systems under a suppression of thermal effect [4,5]. The introducing of photocatalysts as TiO_2 into MW system (TiO_2/MW) exhibited much higher rate than MW irradiation alone and conventional photocatalysis for X-3B decolorization and TOC mineralization [5]. The microwave electrodeless lamp (MWL) shows advantages as high photochemical efficiency, simple photocatalytic equipment and long life [6], and is chosen as light source in this study.

Manganese oxides are widely employed as adsorbents and oxidants for pollutants removal [7,8]. The reductive dissolution of manganese oxides by species that being adsorbed onto manganese surface had been well studied [9–11]. The catalytic effect had also been investigated for manganese oxides and aqueous Mn^{2+} [12–14]. The manganese species impacts the catalytic behaviors and pathways involve in catalysis. Our recent study indicated that Mn^{2+} alone showed weak catalytic effect for ozonation of 2,4-dinitrotoluene (DNT). However, Mn^{2+} coupled with oxalic acid, which converted Mn(IV) to Mn^{2+}, significantly accelerated DNT degradation through cycled catalytic mechanism [15]. Generally, the homogeneous and heterogeneous catalysts exhibit catalytic effects through main mechanisms as [16]: (1) to enhance $^{\bullet}OH$ formation through promoting oxidants (e.g., ozone and H_2O_2) decomposition; (2) to facilitate the formation of highly oxidative species or intermediates which being prone to ozonation. Manganese oxides and manganese-doped catalysts also exhibit photocatalytic activity for organics degradation in aqueous and gas phases [10,11,17,18].

Hydrous manganese dioxide (δMnO_2) exhibits good capabilities for organics adsorption [19]. Additionally, the electron

* Corresponding author.
E-mail addresses: liuruiping@rcees.ac.cn (R. Liu), jhqu@rcees.ac.cn (J. Qu).

0920-5861/$ – see front matter © 2008 Elsevier B.V. All rights reserved.
doi:10.1016/j.cattod.2008.08.035

transfer between organics and δMnO_2 contributes to Mn^{2+} dissolution [9,11]. These two effects are valuable for organics removal. However, rare studies employ δMnO_2 as an adsorbent and catalyst to investigate these combined effects for organics removal and mineralization.

The objectives of this study are: (1) to employ the azo dye of cationic blue (X-GRL) as model pollutant to investigate the oxidative and adsorptive behaviors of δMnO_2, and the commercial MnO_2 (βMnO_2) is chosen as a control adsorbent to compare the reactivity to X-GRL; (2) to propose the interactions between X-GRL and δMnO_2 basing on pH and Ca^{2+} effects analysis; (3) to investigate the adsorptive and catalytic activities of δMnO_2 in O_2/MWL systems for X-GRL degradation and mineralization.

2. Experimental

2.1. Reagents

The cation blue X-GRL (482 g/mol) (Shanghai Huacai Fine Chemicals Co. Ltd.) and βMnO_2 (Beijing Beihua Fine Chemicals Co. Ltd.) were directly used without pretreatment.

δMnO_2 was prepared through reactions between Mn^{2+} by MnO_4^-, following procedures reported by Murray [20]. X-ray diffraction (XD-3A) (Shimadzu Co., Japan) analysis showed low degree of crystallinity, indicating its similarity to what others referred to as δMnO_2.

2.2. Experimental procedures

Batch adsorption experiments were conducted in capped triplicate in darkness with continuous rotary shaking (130 r/min) at 25 ± 1 °C for 120 min. The initial X-GRL concentration was 200 mg/L and pH was determined to be 4.5. pH adjustment was not preceded except when investigating the effect of pH on X-GRL adsorption. $CaCl_2$ was pre-added to 5 mM while investigating Ca^{2+} effect.

The reactor for MWL assisted photodegradation experiments was designed and installed following what Zhang et al. reported [3]. Solution temperature was kept at 45 ± 2 °C through circulating solution to a water cooler with peristaltic pump. Pure oxygen (>99.9%, Beijing Dongfang Oxygen Gas Co.) was introduced to the bottom of the reactor and then evenly dispersed with a sand aerator. The power of the MWL was calculated to be 28.1 W [3].

2.3. Analysis

Samples were filtered through 0.45 μm membranes before analysis. UV–vis spectra were recorded from 190 to 800 nm using a U-3010 UV–vis spectrophotometer (Hitachi Co., Japan). Total organic carbon (TOC) was analyzed by UV-persulfate oxidation with a TOC Analyzer (Phoenix 8000) (Tekmar–Dohrmann Co.). Mn concentration was determined using an atomic absorption spectrophotometer (Z-6100) (Hitachi Co., Japan).

3. Results and discussion

3.1. The adsorptive and oxidative behaviors of X-GRL for δMnO_2 and βMnO_2

3.1.1. UV–vis decrease

Fig. 1 presented the evolution of the UV–vis absorption spectrum of X-GRL at different dosages of βMnO_2 and δMnO_2. X-GRL showed three respective absorption peaks at wavelengths of 202, 300 and 610 nm, which were mainly attributed to the benzene ring, azo linkage or the multi-peaks of the functions within X-GRL. βMnO_2 adsorption contributed to UV–vis absorption decrease at different wavelengths, but to a much lower extent than δMnO_2 did. Quantitatively, βMnO_2 (3.75 g/L) and δMnO_2 (0.41 g/L) contributed to $A_{610\ nm}$ removal of 40.0 and 98.9%, which corresponded to $A_{610\ nm}$ removal potential (removed $A_{610\ nm}$ at per gram MnO_2) of 1.5 and 33.2 L (g cm)$^{-1}$, respectively. Our former studies reported that δMnO_2 exhibited higher adsorbing potential for pollutants as humic acid and arsenite than βMnO_2 did, which was ascribed to its lower particle diameter and higher reactivity [19].

Additionally, the spectra feature variation was investigated for X-GRL. As for X-GRL, the ratio of absorption at different wavelengths of 202, 300 and 610 nm ($A_{202\ nm}/A_{300\ nm}/A_{610\ nm}$) was 1/0.24/2.04. By contrast, the ratio after βMnO_2 (3.75 g/L) adsorption was $A_{202\ nm}/A_{300\ nm}/A_{610\ nm}$ = 1/0.22/1.84, and that after δMnO_2 (0.41 g/L) adsorption was $A_{202\ nm}/A_{300\ nm}/A_{610\ nm}$ = 1/0.10/0.07, respectively. The more significant decrease of $A_{300\ nm}$ and $A_{610\ nm}$ indicated the more complete degradation of corresponsive feature functions (e.g., azo linkage). Generally, δMnO_2 contributed to more significant UV–vis absorption decrease than βMnO_2 did, ascribing to its higher oxidizing capability towards X-GRL.

3.1.2. Dissolved organic carbon (DOC) removal

The DOC removal by βMnO_2 and δMnO_2 adsorption was compared (Fig. 2). As being similar to UV–vis absorption, δMnO_2 showed higher potential for DOC removal than βMnO_2 did. DOC removal potential (removed DOC at per gram MnO_2) was 0.31 and 4.92 mg/g for βMnO_2 and δMnO_2, respectively. δMnO_2 exhibited DOC adsorbing potential of about 15 times higher than βMnO_2 did.

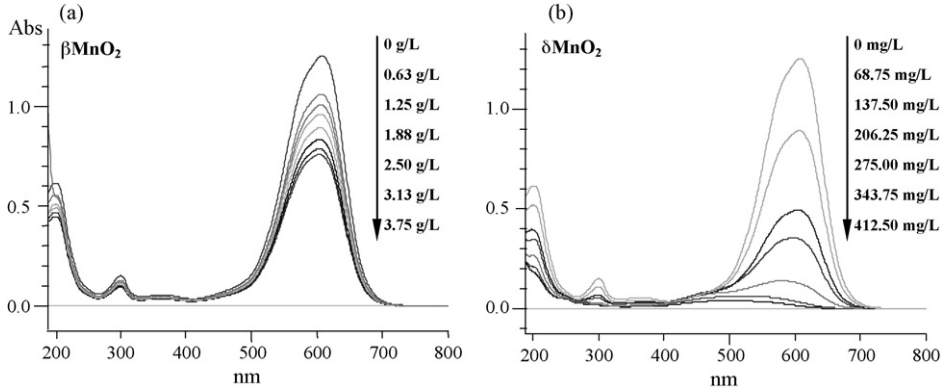

Fig. 1. Comparative adsorbing potential between βMnO_2 (a) and δMnO_2 (b) for X-GRL removal. Experimental conditions: 200 mg/L $[X\text{-}GRL]_0$, pH 4.5, 120 min, 25 ± 1 °C, 130 rpm, samples being diluted to 11 times before UV–vis analysis).

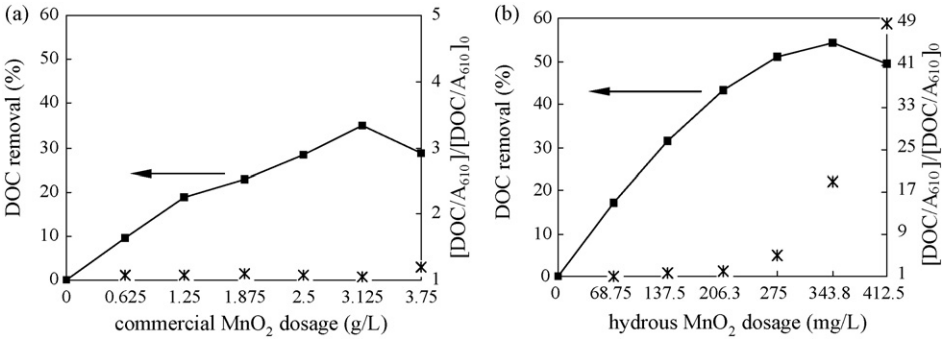

Fig. 2. DOC removal comparison between βMnO_2 (a) and δMnO_2 (b) adsorption. Experimental conditions: 200 mg/L $[X\text{-}GRL]_0$, pH 4.5, 120 min, 25 ± 1 °C, 130 rpm).

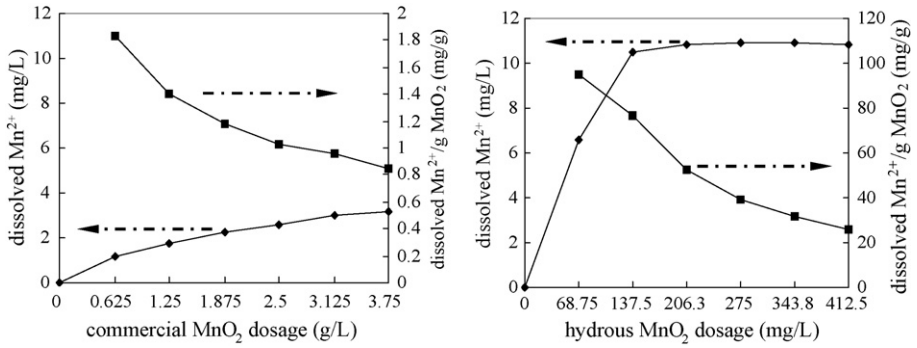

Fig. 3. Comparison of dissolved Mn^{2+} concentration between βMnO_2 (a) and δMnO_2 (b) due to reductive dissolution effects on manganese oxide surfaces. Experimental conditions: 200 mg/L $[X\text{-}GRL]_0$, pH 4.5, 120 min, 25 ± 1 °C, 130 rpm.

The ratio of DOC to $A_{610\ nm}$ ($R_{DOC}/A_{610\ nm}$) after adsorption increased with higher manganese oxides dosages, and more remarkable $R_{DOC}/A_{610\ nm}$ increase was observed for δMnO_2 adsorption. Before adsorption, the $R_{DOC}/A_{610\ nm}$ was 3.10 (mg cm)/L for X-GRL. After adsorption onto βMnO_2 (3.75 g/L) and δMnO_2 (0.41 g/L), $R_{DOC}/A_{610\ nm}$ shifted to 3.69 and 160.8 (mg cm)/L, respectively. $R_{DOC}/A_{610\ nm}$ variation also illustrated the breakage of azo linkage due to manganese oxides oxidation.

3.1.3. Manganese reductive dissolution

The aqueous Mn^{2+} concentration increase further confirmed the oxidation of X-GRL on MnO_2 surface (Fig. 3). Dissolved Mn^{2+} concentration increased with higher MnO_2 dosages, and, respectively, reached a maximum value of 3.2 mg/L (βMnO_2) and 10.9 mg/L (δMnO_2). Mn^{2+} concentration kept constant at δMnO_2 dosage higher than 137.5 mg/L, which seemed that X-GRL did not further react with δMnO_2. However, the UV–vis absorption decrease (Fig. 1b) and the $R_{DOC}/A_{610\ nm}$ increase (Fig. 2b) indicated the occurrence of interactions between X-GRL and δMnO_2 at high δMnO_2 dosages. This conflict was ascribed to the Mn^{2+} readsorption and the formation of complexes between Mn^{2+} and surface-bound X-GRL (and its intermediates) [11].

The adsorption of different pollutants onto manganese oxides and their effects on manganese oxides reductive dissolution had been well studied. Stone [10] studied the adsorption and electron transfer of 27 aromatic and nonaromatic compounds onto Mn(III, IV) oxide suspension, and reported the Mn^{2+} concentration increase. Manning et al. [8] reported the oxidation of As(III) to As(V) on synthetic birnessite surfaces through heterogeneous oxidation mechanisms. The highly reductive functional groups (e.g., azo linkage) within X-GRL contributed to manganese(IV) oxides reduction and Mn^{2+} dissolution after electron transfer.

3.2. Proposed interactions between X-GRL and δMnO_2 basing on pH and Ca^{2+} effects analysis

3.2.1. pH effect

Fig. 4 presented the removal of DOC and $A_{610\ nm}$ by δMnO_2 at different pH. Higher $A_{610\ nm}$ removal was observed at lower pH, owing to the combined effects of adsorption and oxidation. δMnO_2 showed higher reactivity to X-GRL in lower pH ranges, as being indicated from the dissolved Mn^{2+} concentration at pH 2.0 (38.0 mg/L) and pH 11.3 (2.1 mg/L). The higher $R_{DOC}/A_{610\ nm}$ value at lower pH also demonstrated this (Fig. 4). In low pH conditions, hydrogen bonding between hydrogen bond within X-GRL and manganese hydroxyl groups (Mn–OH) dominated X-GRL adsorption onto δMnO_2. Additionally, DOC removal at pH 1.0 (16.7%) was

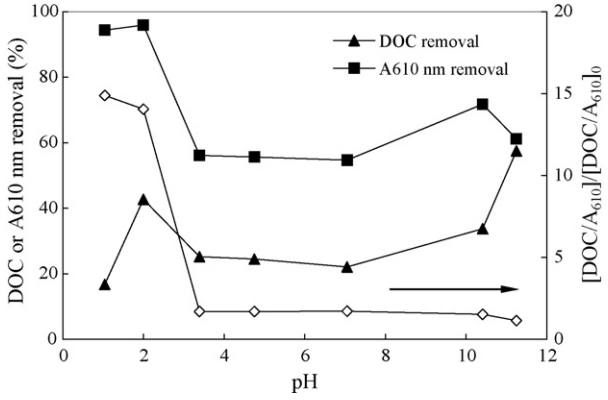

Fig. 4. The adsorption and species transformation of X-GRL onto δMnO_2 at different pH conditions. Experimental conditions: 200 mg/L $[X\text{-}GRL]_0$, 251.8 mg/L δMnO_2, 120 min, 25 ± 1 °C, 130 rpm).

lower than that at pH 2.0 (42.7%). This was due to the formation of intermediate species that being more difficult to adsorb onto δMnO_2 after X-GRL degradation. Actually, after being oxidized by permanganate (pH 2.0), DOC removal by δMnO_2 decreased from 42.7 to 29.5%.

DOC removal was relatively low in pH ranges from 3 to 8, and then increased at pH above 10. The pH_{ZPC} (zero point of charge) of δMnO_2 was near to pH 3 [19]. The ξ potential of δMnO_2 decreased with higher pH, and reached low as −53.5 mV at pH 10.7 [21]. The lower ξ potential benefited the adsorption of positive X-GRL onto δMnO_2.

3.2.2. Ca^{2+} effect

Fig. 5 presented the effect of Ca^{2+} on $A_{610\,nm}$ removal and δMnO_2 dissolution in pH ranges from 1.0 to 11.3. Ca^{2+} presence decreased dissolved Mn^{2+} concentration, indicating its inhibiting effect on δMnO_2 dissolution. Ca^{2+} would complex with Mn–OH and increase its surface charge [19]. The higher surface charge inhibited positively charged X-GRL adsorption and electron transfer between X-GRL and δMnO_2.

3.2.3. Proposed interactions between X-GRL and δMnO_2

Based on the above analysis, the interactions between X-GRL and δMnO_2 were proposed to mainly include reactions from Eq. (1)–(12). For more clear expression, X-GRL equaled to H–(X-GRL)′ or R–N = N–R′ and δMnO_2 was also expressed as MnOH or Mn(IV)OOH.

(1) δMnO_2 surface dissolution and hydrolysis

$$pH < pH_{ZPC}: \quad MnOH + H^+ \leftrightarrow MnOH_2^+ \tag{1}$$

$$pH > pH_{ZPC}: \quad MnOH + OH^- \leftrightarrow MnO^- + H_2O \tag{2}$$

(2) X-GRL adsorption onto δMnO_2

$$pH < pH_{ZPC}: \quad MnOH_2^+ + \text{X-GRL} \leftrightarrow MnOH_2^+ \text{—H-(X-GRL)′(hydrogenbonding)} \tag{3}$$

$$pH > pH_{ZPC}: \quad MnO^- + \text{X-GRL} \leftrightarrow \text{MnO—X-GRL(electrostaticinteraction)} \tag{4}$$

(3) X-GRL oxidation and δMnO_2 dissolution through electron transfer

$$\text{Mn(IV)OO—X-GRL} + 4H^+ \rightarrow Mn^{2+} + \text{R—N} + \text{N—R′} + 2H_2O \tag{5}$$

$$\text{Mn(IV)OO—X-GRL} + 2H^+ \rightarrow Mn^{2+} + \text{intermediates}_{\text{X-GRL}} + H_2O \tag{6}$$

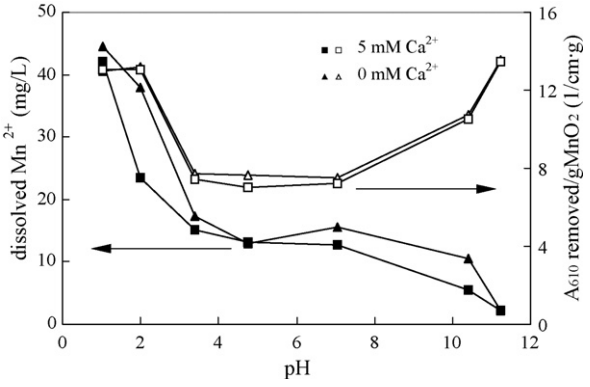

Fig. 5. Effect of Ca^{2+} on X-GRL adsorption and Mn^{2+} dissolution at different pH conditions. Experimental conditions: 200 mg/L $[X\text{-}GRL]_0$, 251.8 mg/L δMnO_2, 5 mM $CaCl_2$, 120 min, 25 ± 1 °C, 130 rpm.

$$\text{Mn(IV)O—OH} + \text{R—N(orN—R′)} + H^+ \rightarrow Mn^{2+} + \text{intermediates}_{\text{X-GRL}} + H_2O \tag{7}$$

(4) Adsorption and electron transfer of X-GRL intermediates onto δMnO_2 surfaces

$$MnOH + \text{R—N(orN—R′)} \rightarrow \text{MnOH—N—R(orMnOH—N—R′)} \tag{8}$$

$$\text{Mn(IV)OO—N—R(orMn(IV)OO—N—R′)} + 2H^+ \rightarrow Mn^{2+} + \text{intermediates}_{\text{N—R(orN—R′)}} + H_2O \tag{9}$$

(5) Surface complexation of Ca^{2+} and dissolved Mn^{2+} onto δMnO_2 surfaces

$$Ca^{2+} + 2MnOH \rightarrow (MnO)_2\text{—Ca} + 2H^+ \tag{10}$$

$$Mn^{2+} + 2MnOH \rightarrow (MnO)_2\text{—Mn} + 2H^+ \tag{11}$$

(6) Ligand exchange between X-GRL and Ca^{2+}

$$2\text{MnO—X-GRL} + Ca^{2+} \rightarrow (MnO)_2\text{—Ca} + 2\text{X-GRL} \tag{12}$$

3.3. Microwave assisted photocatalysis for X-GRL degradation and DOC removal

3.3.1. X-GRL degradation and decolorization

The degradation of dyes in MW systems was often approximated as pseudo-first-order kinetics as the following equation [5]:

$$r = \frac{-dC}{dt} = k_{app}C \tag{13}$$

where r (mg (L min)$^{-1}$) was the rate of X-GRL decolorization and degradation, k_{app} was the apparent reaction constant (min^{-1}) of pseudo-first-order reaction. Whose integration gives, for $C = C_0$ at $t = 0$:

$$-\ln\left(\frac{C}{C_0}\right) = k_{app}t \tag{14}$$

The k_{app} values with different catalysts (δMnO_2, βMnO_2 and Mn^{2+}) presence and control system (with no manganese species presence) for X-GRL decolorization at different wavelengths were presented in Table 1. Functional groups showing absorption at 610 nm (azo linkage) were more easily degraded than those at 202 and 300 nm. The introducing of these catalysts enhanced X-GRL decolorization, with k_{app} being 1.9–5.3 times higher than that of control system. The positive effect of Mn^{2+} implied the effectiveness of dissolved Mn^{2+} from manganese(IV) oxides on X-GRL degradation. Additionally, the heterogeneous systems involved both adsorption and oxidation effects, which showing lower R^2 values than those of homogeneous systems.

Table 1 signified that δMnO_2 exhibited no predominance for catalyzing X-GRL decolorization in comparing to βMnO_2 and Mn^{2+}.

Table 1
Apparent reaction constants (k_{app}) of X-GRL decolorization in O_2/MWL in 120 min

Systems	$A_{202\,nm}$		$A_{300\,nm}$		$A_{610\,nm}$	
	k_{app} (min^{-1})	R^2	k_{app} (min^{-1})	R^2	k_{app} (min^{-1})	R^2
Control	0.0071	0.9886	0.0092	0.9914	0.0191	0.9945
δMnO_2	0.0137	0.7531	0.0188	0.7329	0.0416	0.6771
βMnO_2	0.0189	0.8573	0.0406	0.9982	0.0684	0.8977
Mn^{2+}	0.0174	0.9755	0.0414	0.9665	0.0664	0.9220

Experimental conditions: 200 mg/L $[X\text{-}GRL]_0$, 0.28 g/L δMnO_2, 0.55 g/L βMnO_2, 6.2 mg/L Mn^{2+}, 0.3 L/min O_2, 45 ± 2 °C.

Table 2
k_{app}–$A_{610\ nm}$ comparison for X-GRL decolorization in different reacting periods in O_2/MWL

Systems	0–10 min		10–60 min		60–120 min		0–120 min	
	k_{app} (min^{-1})	R^2	k_{app} (min^{-1})	R^2	k_{app} (min^{-1})	R^2	k_{app} (min^{-1})	R^2
δMnO_2	0.4339	0.8891	0.0173	0.8126	0.0163	0.3869	0.0684	0.8971
βMnO_2	0.1726	0.9646	0.0767	0.9618	0.0250	0.9116	0.0416	0.6771
Mn^{2+}	0.1044	0.9932	0.0904	0.9272	0.0373	0.9704	0.0664	0.9220

Experimental conditions: 200 mg/L $[X\text{-}GRL]_0$, 0.28 g/L δMnO_2, 0.55 g/L βMnO_2, 6.2 mg/L Mn^{2+}, 0.3 L/min O_2, 45 ± 2 °C.

However, the tracking of the k_{app} ($A_{610\ nm}$) during different reacting periods indicated remarkable decolorization in the initial 10 min for δMnO_2 (Table 2). This was due to the combined effects of adsorption, oxidation, and catalysis. The k_{app} (0–10 min) with δMnO_2 presence was about 2.5 and 4.2 times higher than that of βMnO_2 and Mn^{2+}, respectively. With reactions continuing, the release of adsorbed X-GRL (or intermediates) from δMnO_2 surfaces decreased k_{app} values.

3.3.2. DOC removal

DOC removal under different systems was also investigated (Fig. 6). MWL alone showed low capability for DOC mineralization, only achieving 8.8% decrease within 118 min. Under heterogeneous catalytic systems, DOC removal showed rapid increase with subsequent lower rate. The maximal DOC removal was 78.4 and 76.9% for the $\delta MnO_2/O_2$/MWL and $\beta MnO_2/O_2$/MWL systems. With homogeneous Mn^{2+} presence (6.2 mg/L), DOC removal was lower than that of heterogeneous systems in the initial 50 min. Then, DOC removal indicated notable increase, reaching a maximum value of 83.2% at 107 min. The inhibited DOC mineralization in the afterward period ($\delta MnO_2/O_2$/MWL system) was similar to that for X-GRL decolorization in Table 2.

The trends of Mn^{2+} concentrations variation provided valuable information for more clear views involved in these catalytic processes. First, O_2/MWL system activated the oxides surfaces. In comparing to solely reacting with X-GRL, O_2/MWL system favored manganese(IV) oxides dissolution, resulting in maximal value of 318.8 mg/g δMnO_2 and 36.5 mg/g βMnO_2. On the other hand, oxidant species (e.g., H_2O_2, O_3, $^{\bullet}OH$, $O_2^{\bullet-}$) were generated in O_2/MWL system, with more H_2O_2 formation at longer time [3]. These oxidants would then be captured and consumed by Mn^{2+}, transferring Mn(II) to Mn(III, IV) whose capability for DOC mineralization was low (the following equations).

$$Mn(II) \rightarrow Mn(III) + e^- \quad (15)$$

$$Mn(II) \rightarrow Mn(IV) + 2e^- \quad (16)$$

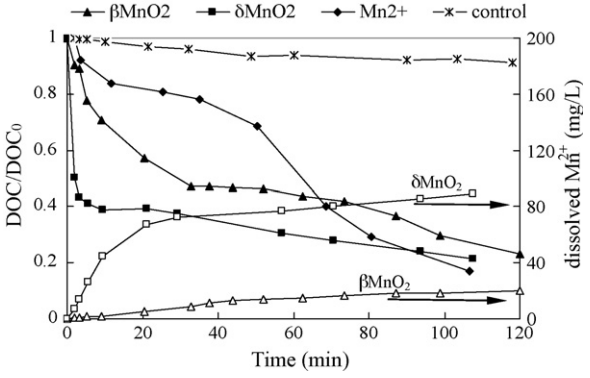

Fig. 6. Trends of DOC removal and Mn^{2+} dissolution under different catalytic O_2/MWL systems. Experimental conditions: 200 mg/L $[X\text{-}GRL]_0$, 0.28 g/L δMnO_2, 0.55 g/L βMnO_2, 6.2 mg/L Mn^{2+}, 0.3 L/min O_2, 45 ± 2 °C.

Additionally, Mn(II) readsorbed onto oxides surface would additionally cause surface deactivation or "poisoning" [11], inhibiting its catalytic effects and possibly adsorptive capabilities for DOC mineralization. These two effects inhibited DOC removal in heterogeneous systems, especially in the afterward periods with high Mn^{2+} concentration.

Comparatively, the Mn(II) in Mn^{2+}/O_2/MWL enhanced the formation of active species as $^{\bullet}OH$ for DOC mineralization through homogeneous catalysis effect. With reactions continuing and more oxidizing species formation, more remarkable DOC mineralization was observed.

4. Conclusions

Manganese oxides show capability for X-GRL adsorption and oxidation, and the freshly prepared δMnO_2 exhibits higher reactivity than βMnO_2 does. Ca^{2+} presence inhibits whereas the higher pH favors positive charged X-GRL adsorption on δMnO_2. During X-GRL adsorption onto manganese oxides, hydrogen bonding and electrostatic interaction are involved. The electron transfer also occurs between oxides surface and X-GRL, which contributes to X-GRL decolorization and manganese(IV) dissolution to Mn(II). In O_2/MWL system, the combined effects of adsorption and catalysis enhance X-GRL degradation and DOC removal when δMnO_2 and βMnO_2 are present, and more positive effects are observed in the initial 60 min. However, DOC removal decreases and the dissolved Mn^{2+} concentrations increase greatly in the upper periods. The high Mn^{2+} concentration in the $\delta MnO_2/O_2$/MWL and $\beta MnO_2/O_2$/MWL systems exhibits adverse effects for DOC mineralization, in comparing to the Mn^{2+}/O_2/MWL system.

Acknowledgements

This work was supported by the Funds for the Creative Research Groups of China (Grant No. 50621804). Appreciation is extended to the foundation for financial assistance.

References

[1] S. Kataoka, D.T. Tompkins, W.A. Zelter, M.A. Anderson, J. Photochem. Photobiol. A: Chem. 148 (2002) 323–330.
[2] S. Horihoshi, H. Hidaka, N. Serpone, Environ. Sci. Technol. 36 (2002) 1357–1366.
[3] X. Zhang, G. Li, Y. Wang, J. Qu, J. Photochem. Photobiol. A: Chem. 184 (2006) 26–33.
[4] D.H. Han, S.Y. Cha, H.Y. Yang, Water Res. 38 (2004) 2782–2790.
[5] X. Zhang, G. Li, Y. Wang, Dyes Pigments 74 (2007) 536–544.
[6] P. Klan, J. Literak, M. Hajek, J. Photochem. Photobiol. A: Chem. 128 (1999) 145–149.
[7] Z. Ma, L. Dong, Y. Kang, L. Jiang, Tech. Equip. Environ. Pollut. Cont. 3 (2002) 19–22.
[8] B. Manning, S. Fendorf, B. Bostick, D. Suarez, Environ. Sci. Technol. 36 (2002) 976–981.
[9] A. Stone, Environ. Sci. Technol. 21 (1987) 979–988.
[10] A. Stone, J. Morgan, Environ. Sci. Technol. 18 (1984) 617–624.
[11] R. Petrie, P. Grossl, R. Sims, Environ. Sci. Technol. 36 (2002) 3744–3748.
[12] R. Andreozzi, V. Caprio, A. Insola, Water Res. 32 (1998) 1492–1496.
[13] J. Ma, N. Graham, Water Res. 33 (1999) 785–793.

[14] J. Ma, M. Sui, T. Zhang, C. Guan, Water Res. 39 (2005) 779–786.
[15] H. Xiao, R. Liu, X. Zhao, J. Qu, J Mol Catal A Chem. 286 (2008) 149–155.
[16] K. Barbara, Z. Maria, N. Jacek, Appl. Catal. B: Environ. 46 (2003) 639–669.
[17] R. Jothiramalingam, M. Wang, J. Hazard. Mater. 147 (2007) 562–569.
[18] J. Villaseñor, P. Reyes, G. Pecchi, Catal. Today 76 (2002) 121–131.
[19] R. Liu, Y. Yang, G. Li, W. He, H. Han, Front. Environ. Sci. Eng. China 1 (2007) 1–6.
[20] J. Murray, J. Colloid Interf. Sci. 46 (1974) 357–371.
[21] R. Liu, Y. Yang, S. Xia, W. He, H. Han, G. Li, Environ. Chem. 24 (2005) 338–339.